BASIC SCIENCE

Nanomedicine: Nanotechnology, Biology, and Medicine
11 (2015) 1915–1924

Original Article

nanomedjournal.com

Biodistribution, excretion, and toxicity of mesoporous silica nanoparticles after oral administration depend on their shape

Linlin Li, PhD*, Tianlong Liu, PhD, Changhui Fu, MD, Longfei Tan, PhD, Xianwei Meng, PhD, Huiyu Liu, PhD*

Laboratory of Controllable Preparation and Application of Nanomaterials, Technical Institute of Physics and Chemistry, Chinese Academy of Sciences, Beijing P. R. China

Received 28 January 2015; accepted 3 July 2015

Abstract

Mesoporous silica nanoparticles (MSNs) have been proven to be effective drug carriers for oral delivery. However, little attention has been paid to their *in vivo* biodistribution and toxicity after oral administration. The effect of particle shape on their *in vivo* behavior is also unknown. In this study, we systematically studied the acute toxicity and biodistribution of three types of MSNs with aspect ratios (ARs) of 1, 1.75 and 5 after oral administration. The effect of particle shape as a key physicochemical parameter of MSNs was discussed. With the increase of AR, MSNs showed decreased *in vivo* biodegradation, systematic absorption and excretion, especially decreased liver distribution and urinal excretion. During the period of urinal excretion, MSNs induced a shape-dependent renal damage including hemorrhage, vascular congestion and renal tubular necrosis. These findings will enrich the knowledge to rationally engineer bionanomaterials, and bring new insights into nanotoxicity.

From the Clinical Editor: Advances in nanotechnology have resulted in improvement in drug delivery, of which mesoporous silica nanoparticles have been used as carriers for oral drugs. Nonetheless, studies on their absorption, distribution, metabolism, excretion (ADME) and toxicity still need to be performed. In this article, authors evaluated the effects of particle size and shape on in vivo behavior. The findings would shine light on future design of future drug delivery systems.

Key words: Mesoporous silica nanoparticles (MSNs); Shape; Biodistribution; Oral administration; Toxicity

Engineered nanoparticles have shown potentials in revolutionizing medical practice by enabling real-time diagnosis, high-sensitive biomedical imaging, and targeted drug delivery.[1,2] The expanding applications of nanoparticles in modern medicine require a thorough understanding of their *in vitro* and *in vivo* behaviors.[3] Elucidating the *in vivo* absorption, distribution, metabolism, excretion (ADME) and toxicity of nanoparticles could bring better insight into toxicological profile of these nanoparticles. To improve the drug solubility and bioavailability while protecting the drugs from biodegradation, various nanoparticle-based drug delivery systems have been developed.[4,5] The drugs are usually administered by oral route since it is the most convenient, inexpensive and non-invasive route for patients.

Mesoporous silica nanoparticles (MSNs) as one of the most promising drug delivery carriers have attracted increasing attention.[6-11] It is worth noting that fabrication of MSNs is simple, cost-effective and controllable.[12] The high surface area and large pore volume of this material allow it to be used for encapsulating various therapeutic agents with high loading capacity and delivering them to desired locations.[13-17] They have also been proven to be effective for oral drug delivery especially for water insoluble drugs, inducing significantly enhanced oral bioavailability.[18-21]

It is well known that physicochemical characteristics of nanoparticles including size, shape, surface chemistry and structure all play important roles in determining their *in vitro* and *in vivo* behavior. Particle shape was found to influence the cellular uptake, *in vivo* biodistribution,[22] the flow and adhesion in the vasculature[23] and angiogenesis.[24] For instance, nanorods were reported to show reduced phagocytosis and longer *in vivo* circulation time.[25-27] These studies suggest that understanding

Conflict of interest statement(s), disclosure(s), and/or financial support information, including donations: The authors have no conflicts of interest, and have nothing to disclose. This work received financial support from the National Natural Science Foundation of China (NSFC) (No. 31270022, No. 81471784, No. 31271075, No. 51572271 and No. 51202260).

*Corresponding authors at: Technical Institute of Physics and Chemistry, Chinese Academy of Sciences, Beijing, P. R. China.

E-mail addresses: linlinli@mail.ipc.ac.cn (L. Li), liuhy@mail.ipc.ac.cn (H. Liu).

http://dx.doi.org/10.1016/j.nano.2015.07.004
1549-9634/

the effect of shape on *in vivo* kinetics and biocompatibility is essential to improve the performance of nanomedicine. Although there exist several studies on the biological effects of MSNs related to particle shape,[28-30] these studies are mainly focused on cellular uptake and *in vivo* toxicity after intravenous administration. Very little is known about *in vivo* ADME and toxicity of particles after oral administration.[21] The effects of specific physicochemical characteristics of MSNs, which would significantly influence their interaction with body and their performance as drug carriers, have also rarely been studied.

In the present study, MSNs with three different aspect ratios (ARs = 1, 1.75 and 5) were synthesized and their *in vivo* biodistribution and toxicity after oral administration were systematically evaluated. The *in vivo* biodistribution and excretion of these MSNs were measured at different time intervals by ICP-OES. The acute toxicity of the different shaped MSNs was systematically evaluated. *In vitro* biodegradation of MSNs was found to be consistent with their *in vivo* behavior. These findings are of significance for better design MSNs as oral drug carriers.

Methods

Materials

Cetyltrimethylammonium bromide (CTAB), tetraethyl orthosilicate (TEOS), $NH_3{\cdot}H_2O$ (28%–30%) and sodium dodecylsulfate (SDS) were obtained from Beijing Chemical Reagents Company. Sodium azide, hematoxylin and eosin were purchased from Sigma.

Fabrication of the MSNs with different aspect ratios

The different shaped MSNs were synthesized using a method modified from a previous report.[30] Briefly, cetyltrimethylammonium bromide (CTAB) was dissolved in 70 mL of H_2O followed by the addition of $NH_3{\cdot}H_2O$ under stirring for 1 h. TEOS was then added under vigorous stirring for another 4 h at room temperature. The molar ratio of CTAB:H_2O:$NH_3{\cdot}H_2O$:TEOS in the reaction mixture was 0.1:1000:10:0.7, 0.18:1000:20:1.4 and 0.5:1000:20:2.8, for spherical particles (AR = 1, denoted as NSs), short-rod MSNs (AR = 1.75, denoted as NSRs) and long-rod MSNs (AR = 5, denoted as NLRs), respectively. Different shaped MSNs were collected by centrifugation at 15,000*g* for 20 min, washed and redispersed several times with deionized water and ethanol, alternatively. Surfactant templates were removed by extraction in acidic ethanol (1 mL of HCl in 50 mL ethanol) for 24 h. Morphology and structure of the obtained MSNs were analyzed by a JEM-2100 transmission electron microscope (TEM).

In vitro biodegradation of the MSNs

The *in vitro* biodegradation experiments were conducted according to our previous report.[31] Simulated gastric fluid (pH = 1.2), simulated intestinal fluid (pH = 6.8) and simulated body fluid (pH = 7) were prepared according to a reference.[32] All the nanoparticles were sterilized by ultraviolet (UV) light treatment for 1 h, followed by immersion in 75% ethanol for 2 h. The *in vitro* biodegradation was performed by immersing the samples into different media at a particle concentration of 2.0 mg mL^{-1} in a sealed sterile polypropylene vial at a constant temperature of 37 °C and a shaking rate of 150 rpm min^{-1}. After 7 days, the suspensions were centrifuged and washed with 10% SDS to detach the adsorbed serum proteins. The residues were weighted for quantifying the biodegradation activity. The biodegradation ratio was calculated using the formula: degradation ratio (%) = $100 \times (W_t - W_r)/W_t$, in which W_t is weight of added MSNs and W_r is weight of residues. The particles before and after degradation were characterized by TEM.

Animals

All animal experiments were performed in compliance with the local ethics committee. Male ICR mice (provided by Weitonglihua Experimental Animal Co., Ltd), aged 6–8 weeks, were used in the experiments. They were acclimated in the controlled environment (temperature: 22 ± 1 °C; humidity: 60 ± 10% and light: 12 h light/dark cycle) with free access to water and commercial laboratory complete food.

In vivo toxicity

Twenty four of healthy male ICR mice were allocated into 4 groups (n = 6): control group, NSs-, NSRs-, and NLRs-treated group. Prior to oral administration, the animals were fasted overnight (>12 h). The MSNs suspension in physiological saline at a dose of 40 mg kg^{-1} and volume of 100 μL was intragastrically administrated using a lavage needle. After administration, the ration, body weight and clinic manifestation were recorded at the time points according to the regulation. At 14 days, blood was drawn for hematology analysis (potassium EDTA collection tube) using a standard saphenous vein blood collection technique. Blood samples collected via the ocular vein (about 0.8–1 mL each mouse) were centrifuged twice at 3000 rpm for 10 min to separate serum. Blood biochemical assay was assayed using a Biochemical Autoanalyzer (Type 7170, Hitachi, Japan). The animals were killed and the coefficients of heart, liver, spleen, lung, kidney and thymus to body weight were calculated as the ratio of tissues (wet weight, mg) to body weight (g). Tissues recovered from the necropsy including liver, kidneys, spleen, lung, heart, brain, testis, thymus, duodenum, jejunum and colon were fixed in 10% formalin, embedded in paraffin, sectioned, and stained with hematoxylin and eosin (H&E) for histological examination using standard techniques. After H&E staining, the slides were observed and micrographs were taken on microscope (Nikon Eclipse Ti-S, CCD: Ri1).

Biodistribution and excretion by ICP-OES

To study the biodistribution of MSNs after oral administration, 36 of healthy male ICR mice were allocated into four groups: control group, NSs-, NSRs-, and NLRs-treated group. The mice were intragastrically administrated with MSNs at a dose of 40 mg kg^{-1}. To measure the biodistribution and excretion of MSNs from urine and feces, special single-mouse metabolic cages were used. After oral administration, urine and feces were collected into separate collection tubes at different

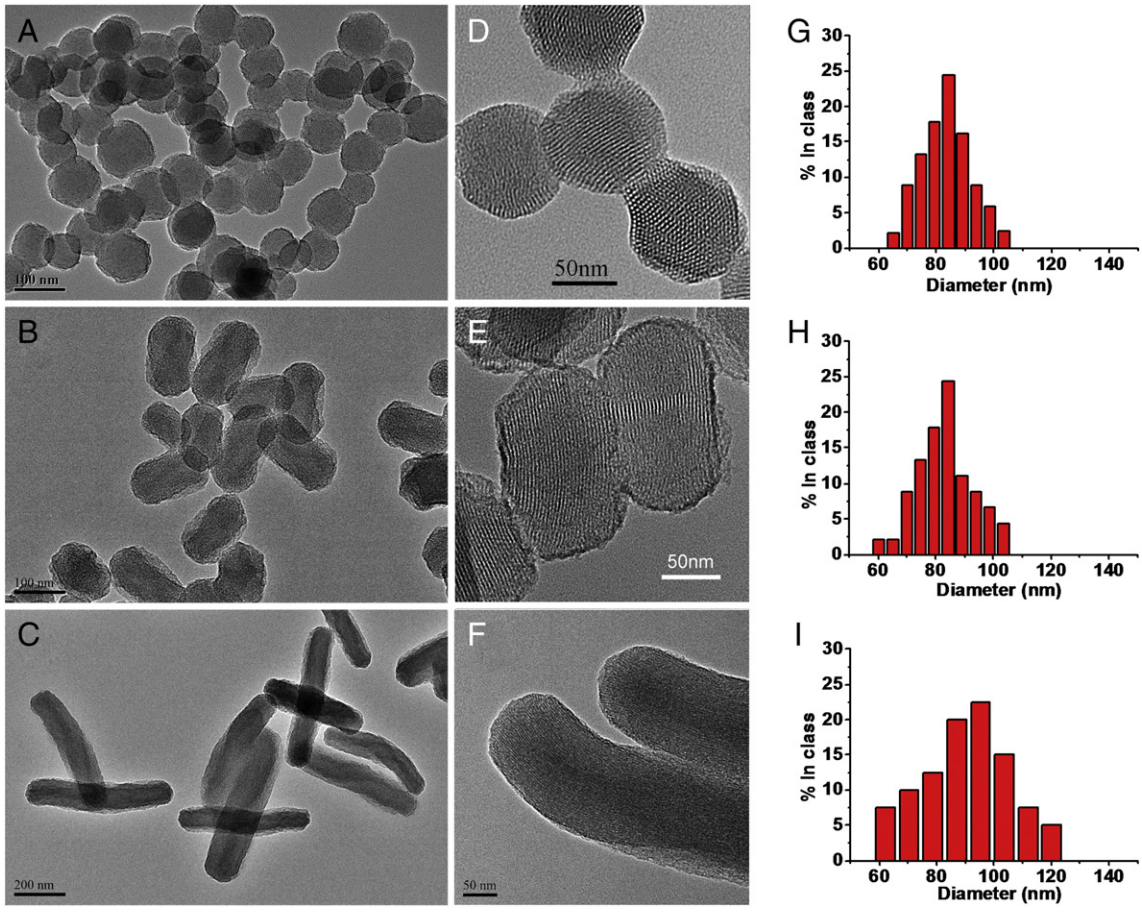

Figure 1. **(A-C)** TEM, **(D-F)** HR-TEM, and **(G-I)** size distribution of **(A, D, G)** sphere-shaped MSNs (NSs), **(B, E, H)** short-rod MSNs (NSRs), and **(C, F, I)** long-rod MSNs (NLRs).

time points. At 2 h, 24 h, and 7 days post-administration, three mice in each group were separately analyzed for tissue Si content. After collection of blood, mice were sacrificed and the following tissues were collected: liver, kidneys, spleen, lungs and small intestines. The small intestines were thoroughly washed with PBS buffer to remove the intestinal content. The wet samples were weighed, digested with nitric acid by heating and then analyzed for silicon content using inductively coupled plasma-optical emission spectrometer (ICP-OES, VARIAN VISTA-MPX, US). The collected urine and feces were also analyzed for Si content by ICP-OES.[33]

TEM imaging of tissues

To determine the localized biodistribution of nanoparticles in tissues, the tissues were observed by bio-TEM. Liver, spleen, duodenum, jejunum and colon tissues were excised at 24 h after MSNs administrated at 40 mg kg^{-1} and immediately fixed in 3% glutaraldehyde overnight. The samples were then treated according to the general protocols for TEM study. The ultrathin sections (60 nm) were stained with lead citrate and uranyl acetate. The sections were viewed on a Hitachi H-7650 TEM operating at 80 kV. Control animals without any treatment were also conduced following the same procedures. All the identity and analysis of the ultrathin section were blind to the pathologist.

Statistics

Data are presented as means ± SD. Analysis of variance and *t* tests were used to analyze the data.

Results

By tuning the molar ratio of TEOS and surfactant CTAB, three different shaped mesoporous silica nanoparticles with a diameter of ca. 85 nm and aspect ratios of 1, 1.75, and 5 were synthesized according to our previously reported method.[30] Figure 1 shows the TEM images and size distributions (calculated from 100 nanoparticles for each sample) of all three MSNs. Spherical-shaped MSNs with AR = 1 (NSs) have an average diameter of 83 nm (Figure 1, *A*, *D*, *G*). Short-rod MSNs (NSRs) (Figure 1, *B*, *E*, *H*) have a similar diameter of 83 nm with a length of about 146 nm and AR of 1.75. Long-rod MSNs (NLRs) (Figure 1, *C*, *F*, *I*) have a slightly larger diameter of about 96 nm with a length of about 483 nm and an AR of 5. Compared with the NLRs, the NSs and the NSRs had relatively smaller diameters and narrower size distributions. All the nanoparticles were monodispersed with high dispersity in aqueous solutions. High-resolution TEM (Figure 1, *D-F*)

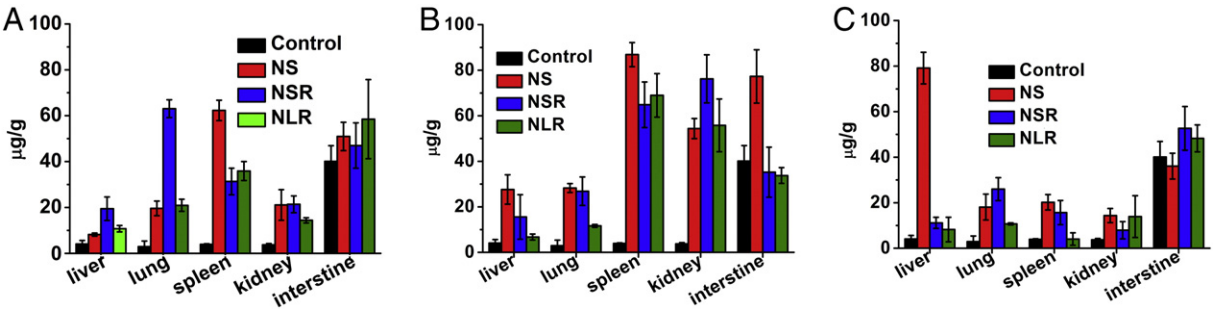

Figure 2. Quantitative analysis of the biodistribution of the MSNs in organs by ICP-OES. Si contents in liver, lung, spleen, kidney, intestine and blood at **(A)** 2 h, **(B)** 24 h and **(C)** 7 days after oral administration.

shows that all the nanoparticles have long-range hexagonal mesoporous structures with an average pore size of about 2.8 nm. The MSNs had similar Zeta potentials within the range of −20 to −25 mV after removal of surfactant CTAB. The similar surface chemistry, diameter, pore size and structure ensure that we can exclusively study the effect of particle shape.

To study the *in vivo* biodistribution of the MSNs after oral administration, the mice were intragastrically administrated with a single dose of 40 mg kg^{-1} MSNs. This dose was also used in our previous research for studying the size effect of MSNs on biodistribution and excretion after intravenous administration.[30] At different time intervals of 2 h, 24 h and 7 days, liver, lung, spleen, kidney, intestine, feces and urine were collected for measuring Si content by ICP-OES. At 2 h post-administration, all three-shaped MSNs had an observable distribution in liver, lung, spleen and kidney (Figure 2, *A*), demonstrating that the MSNs could be intestinally absorbed and then enter into systematic circulation. The NSRs had a higher content in liver and lung, whereas the NSs had a higher content in spleen compared with their counterparts. All three MSNs had a comparable distribution in kidney. In liver and lung, the content of NSRs was about 2-fold and over 3-fold of that of NLRs and NSs, respectively, and in spleen, the content of NSs was about 2-fold of that of NSRs and NLRs. At 24 h post-administration, all the MSNs had a 1.4–2.2 times increased content in spleen and 2.6–3.9 times in kidney (Figure 2, *B*) respectively compared to that of 2 h, but it decreased to a low level at 72 h (Figure 2, *C*). In liver, the content of NSs had a continuous increase from 2 h to 72 h, but their rod-like counterparts had opposite trends. In lung, no obvious difference among the three kinds of MSNs was found. Because the Si content in intestine of control group was very high due to the silicon-containing feed, the distinction in the MSNs-treated groups was not obvious. For the NSs, the Si content in intestine had a one-fold increase at 24 h compared with that of control group, whereas the change was not obvious for the NSRs and NLRs treated animals.

The excretion of the MSNs from the body was also analyzed via detecting the Si content in feces and urine (Figure 3). The three different shaped MSNs showed different trends in the excretion rate from feces and urine. For the control group, Si content in feces was high and fluctuated related to the silicon-containing feed (*i.e.*, above 400 μg g^{-1}), but it was clear that at 2 h post-administration the Si content in feces of the NSs-, the NSRs-, and the NLRs-treated groups was over 2 times higher than the control group. At 24 h and 7 days post-administration, the difference between treatment groups and control groups was not as obvious as that at 2 h post-administration (Figure 3, *A*), demonstrating fast excretion of silica from feces. In urine, the Si content of treatment groups at 2 h was about 1.5–4.3 times higher than that of the control group (Figure 3, *B*). With the increase of aspect ratio from 1 to 5, the Si content in urine at 2 h post administration increased. At 24 h and 7 days post administration, the Si content in treatment groups was only slightly higher than that of control group and the distinction between three treatment groups was not obvious. From these results, it was speculated that most of the oral-administrated MSNs would be rapidly excreted from feces through gastrointestinal tract, but some intact MSNs or their degradation products could be absorbed through intestinal mucosa, entered into systematic circulation, and finally be excreted from body via renal excretion. It should be further clarified why the MSNs with smaller aspect ratios have higher renal excretion.

To further determine the ultrastructural localization of MSNs, tissues including liver, spleen, duodenum, jejunum and ileum were visualized by TEM observation at 24 h post-administration. No histological abnormality was observed in liver and spleen for all the MSNs-treated mice compared to control group (Figure S1). In liver and spleen, we did not find nanoparticles with typical mesoporous structure for all the treatment groups, but we could not exclude the possibility that the MSNs with non-typical nanostructure may be confused with the sub-cellular structure and multiprotein complexes of tissues under low-resolution bio-TEM. Figure 4 shows the TEM images of duodenum, jejunum and ileum of the NSs-treated groups. In the left column image with low resolution, it was found that the tissues had no histological abnormality. With high resolution, spherical particles of ~100 nm, most likely NCs, were found in the cells within the lamina propria of the duodenum (Figure 4, *A*, right column, arrow),. Similarly, in the jejunum (Figure 4, *B*, right column, arrow) and the ileum (Figure 4, *C*, right column, arrow), particles or particle aggregates were also found. In comparison, nonspherical particles NSRs and NLRs were not found in the duodenum, jejunum, or ileum (Figure S2).

It has been proven that MSNs is biodegradable, which is advantageous for their complete drug release and excretion from body after therapy when used as drug carriers.[34-36] The degradation behavior has been found to be related with the inherent physicochemical properties of MSNs, as well as pH,

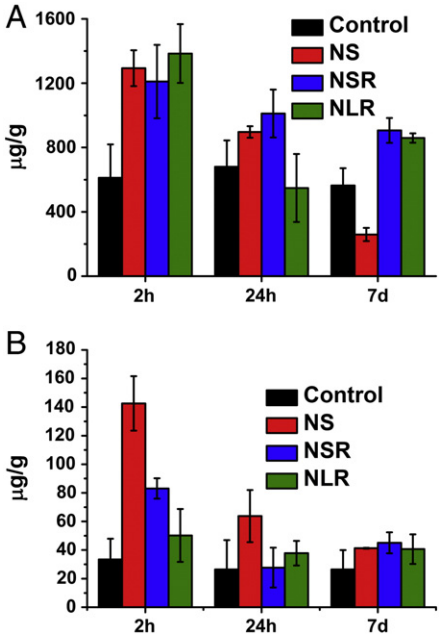

Figure 3. Quantitative analysis of excretion of the MSNs from the body by ICP-OES. Si contents in **(A)** feces and **(B)** urine at different time points.

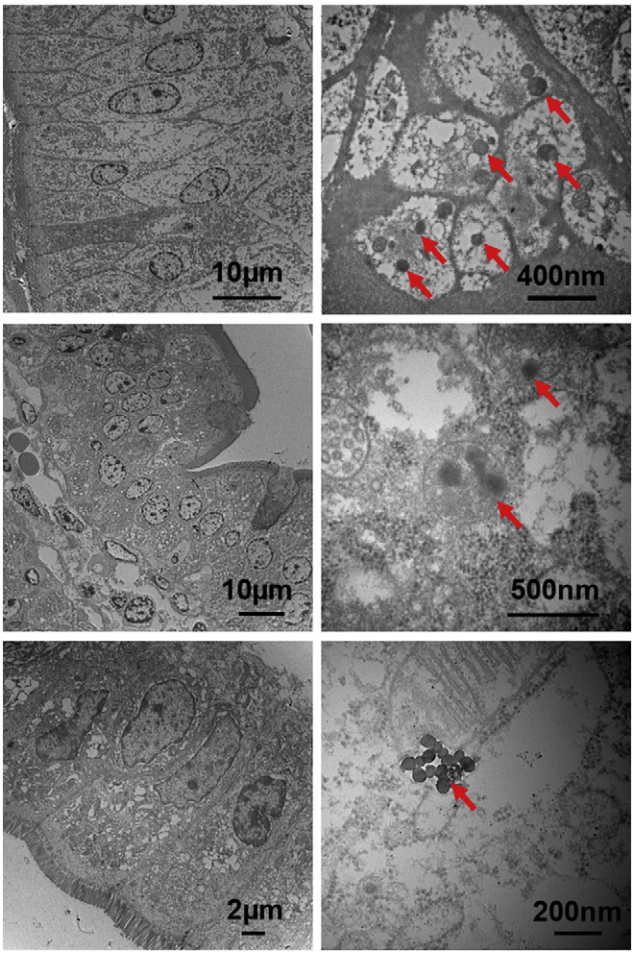

Figure 4. TEM images of **(A)** duodenum, **(B)** jejunum and **(C)** ileum from mice sacrificed at 24 hours post-administration of NSs.

iron and serum *etc* in the environment. Their degradation behavior after oral administration, however, is still unclear. Intuitively, the biodistribution of MSNs and silicon elements should be related with their biodegradation and bioavailability. To better understand the influence of MSNs biodegradation along with their aspect ratio on biodistribution, we examined the nanoparticle stability and biodegradation in a range of *in vitro* simulated fluids. After oral administration, the first environment that the MSNs would encounter is the gastrointestinal tract (GIT). Thus, simulated gastric fluid (pH = 1.2), simulated intestinal fluid (pH = 6.5) and simulated body fluid (pH = 7) were used to investigate the state of different shaped MSNs. After 7 days soak in these simulated fluids, the morphology of MSNs in the three simulated fluids was observed by TEM (Figure 5, *A-I*). The degradation rate was calculated by weighing remanent silica contents after 7 days treatment (Figure 5, *J*). In simulated gastric fluid with an acidic pH, the MSNs with different shapes did not show any obvious change in their morphology or dispersity (Figure 5, *A*, *D*, *G*). However, in simulated intestinal fluid with a nearly neutral pH, significant change was observed. For the NSs with spherical shape, the inner part of the particle had almost been completely corroded, leaving behind a hollow shell, demonstrating that the particles were degraded from inside (Figure 5, *B*). It is possible that the surface of the NSs was protected by multiple ions such as bicarbonate and taurocholate in the fluid and became more resistant to corrosion in the harsh condition. In comparison, the short- and long-rod MSNs were shown to degrade from the surfaces of particles at a slower degradation rate than NSs. In simulated body fluid, all the particles showed a shape-dependent degradation from the surfaces of particles. Although all three MSNs showed low degradation ratio (<10%) in simulated gastric fluid, they became much higher in simulated intestinal and body fluids (Figure 5, *J*). The degradation ratio for NSs, NSR and NLR was 62%, 29% and 17% in simulated intestinal fluid, and 47%, 22%, 17% in simulated body fluid, respectively. The degradation rate was shape-dependent with NSs showing the fastest degradation and NLRs the slowest in all three kinds of simulated fluids. In addition, all MSNs had the slowest degradation in simulated gastric fluid and the fastest degradation in simulated intestinal fluid irrespective of the particle shape. These results suggest that biodegradation of MSNs not only depends on shape but also *in vivo* distribution of the particles, which was advantageous to oral drug delivery. As an oral drug carrier, intact MSNs could protect encapsulated therapeutic agents from the harsh acidic environments in stomach enriching with various enzymes. Once they enter into intestines, the MSN particles start to degrade and the loaded therapeutic agents will then be released, inducing increased drug bioavailability and therapeutic outcomes. From the results shown in Figures 2-5, both the systematic biodistribution and excretion of the MSNs were related to the particle shape and the degradation rate. With an increase in the aspect ratio of MSNs, the degradation rate decreased, and the total Si content in the detected organs (corresponding to the body absorption) decreased accordingly. Meanwhile, the excretion from urines

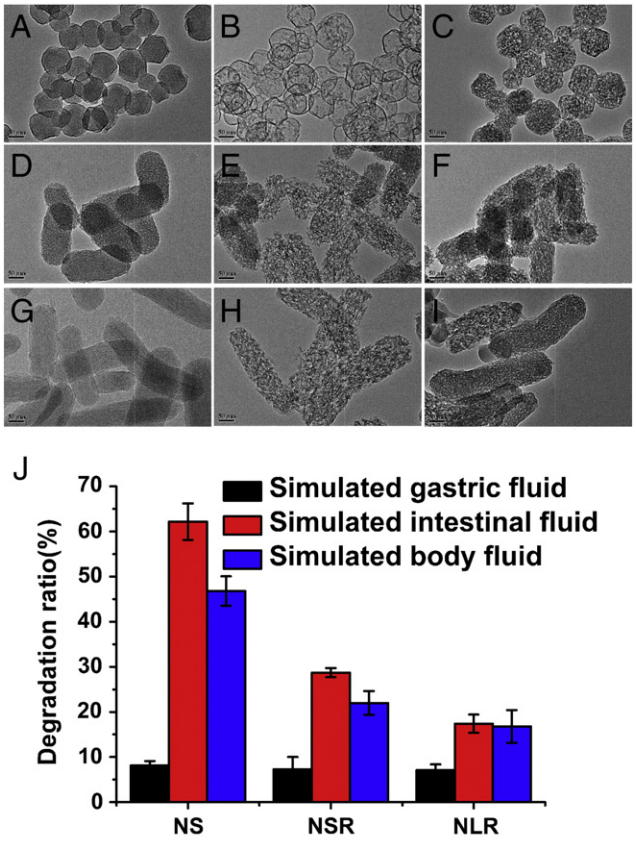

Figure 5. TEM images and calculated degradation rate of the MSNs after biodegradation for 7 days. **(A–C)** NSs, **(D–F)** NSRs, **(G–I)** NLRs in **(A, D, G)** simulated gastric fluid, **(B, E, H)** simulated intestinal fluid, and **(C, F, I)** simulated body fluid. **(J)** Quantitative data of degradation rate.

decreased. All together, these results confirmed that particle shape plays important roles in systematic absorption, biodistribution and excretion of MSNs.

In vivo toxicity after oral administration of different shaped MSNs was detected. During the time course of 14 days, the mice in the control group gained 15% body weight, whereas the NSs-, the NSRs-, and the NLRs-treated groups gained 8.9%, 5.7%, and 6.9% body weight, respectively (Figure S3, *A*). The suppression of body weight gain especially for NSRs and NLRs may come from toxicity of the particles. For the three different shaped MSNs, all coefficient indices including heart, liver, spleen, lung, kidney and thymus showed no obvious change (Figure S3, *B*). In the entire study period, no unusual behaviors were observed for all the animals, including vocalizations, labored breathing, difficulties moving, hunching or unusual interactions with cage mates.

To study the effect of different shaped MSNs on blood, hematology and serum biochemical indicators were measured at 14 days post-administration. Representative serum biochemical indicators including alanine aminotransferase (ALT), aspartate aminotransferase (AST), total bilirubin (TBIL), alkaline phosphatase (ALP), creatinine (CREA), blood urea nitrogen (BUN), dehydrogenase (LDH) and albumin (ALB) were quantified (Figure 6, *A*). No significant changes were observed in the biochemical markers for liver function including ALT and AST. However, the activity of CREA, an indicator of glomerular filtration, increased for all MSNs, with that of the NLRs-treated group exceeding the normal range of ICR mice. Although in a normal range, LDH decreased for the NSs-, NSRs- and NLRs-treated groups compared with that for the control group, suggesting the change in cardiac activity. As a parameter of tissue damage or inflammation, albumin (ALB) content was also measured but showed no difference between the control group and the MSNs-treated groups. No significant changes were observed for ALP and TBIL as markers for biliary function, and BUN as a marker for kidney function for all groups.

Representative red blood cell count (RBC), hemoglobin (HGB), hematocrit (HCT), mean corpuscular volume (MCV), mean corpuscular hemoglobin (MCH), mean corpuscular hemoglobin concentration (MCHC), platelet count (PLT) and white blood cell count (WBC) were also detected (Figure 6, *B*). For all these hematology markers, there was no significant difference between the MSNs-treated groups and the control group, all within the normal range of ICR mice. Other hematologic markers including mean corpuscular hemoglobin (MCH), platelet count (PC), corpuscular hemoglobin concentration (CHC) and mean corpuscular volume (MCV) also did not show any obvious difference among the four groups (data not shown). The results suggest that all three MSNs had no obvious hematological toxicity.

To analyze the toxicity of different shaped MSNs on a microscopic level, major organs from animals were subject to histological evaluation. No histological abnormality such as villus length, lamina propria and muscularis mucosae was observed in the small intestine including duodenum, jejunum and ileum for the three MSNs-treated groups compared with the control group (Figure 7). The histological micro-morphology structure of heart, liver, spleen and lung showed no evident pathological changes as compared to the control group (Figure S4). In addition, brain, thymus and testis did not show any histological abnormalities for all four groups (data not shown).

However, renal tubular necrosis, hemorrhage and vascular congestion in the renal interstitium were observed in the kidney nipple area for all the MSNs-treated mice irrespective of the geometrical features of the MSNs (Figure 8), suggesting the possible kidney damage. These results are consistent with the abnormal level of CREA biochemical marker detected. It was found that the severity of tissue abnormalities was dependent on particle shape, with NSs inducing the most serious kidney damage including hemorrhage and renal tubular necrosis and the lightest damage by NLRs, *i.e.*, only slight hemorrhage.

Discussion

Intestinal epithelial barrier is one of the main natural physiological barriers that can effectively protect the body from dangers.[37] Previously, several studies have found that the absorption of micro-/nano-particles across the intestinal mucous membrane to the circulation was size-dependent after oral administration.[38] Gold nanoparticles with different sizes varying from 1.4 to 200 nm showed size-dependent absorption to the

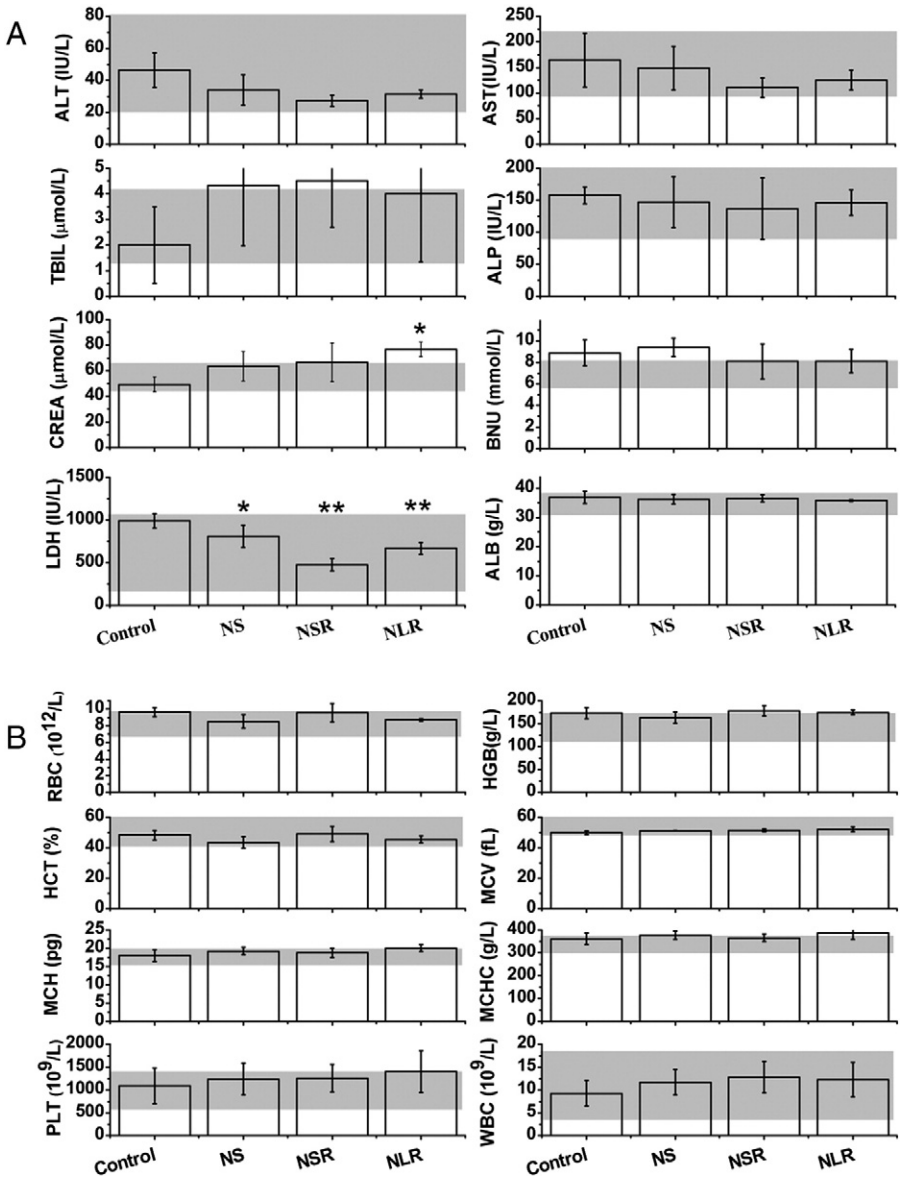

Figure 6. Effect of different shaped MSNs on **(A)** serum biochemistry and **(B)** hematology at 14 d post-administration. Related serum biochemistry indicators include ALT, AST, TBIL, ALP, CREA, BUN, LDH, and ALB. Relative hematology indicators include RBC, HGB, HCT, MCV, MCH, MCHC, PLT and WBC. Gray bars indicate the range of values obtained from healthy ICR mice.

circulation, with higher absorption of smaller particles, but the absorption by the body was very low.[39] Eldridge *et al* found that 5–10 μm biodegradable microspheres remained fixed in the Peyer's patches, while the smaller ones (1–5 μm) were transported through the efferent lymphatics with the macrophages and targeted to liver and spleen passively.[40] Jani *et al* reported that 100–500 nm nondegradable polystyrene spheres were distributed in liver, Peyer's patches, villi, lymph nodes and spleen.[41] From the different distribution tendency of degradable and non-degradable particles, we speculate that the biodegradation behavior of particles has a great influence on their uptake and translocation after oral administration. In this study, biodegradation behavior and shape of the MSNs are two key factors influencing their biodistribution and excretion. Since biodegradation behavior is related to particle shape, shape is believed to be the most important factor in determining their biodistribution and excretion.

Previously, we have studied the effect of shape of MSNs on *in vivo* biodistribution after intravenous injection and showed that the Si content in liver and urine decreased with the increase of aspect ratio from 1.5 to 5.[30] Herein, similar shape-dependent liver distribution and urine excretion of MSNs were observed after oral administration. However, the distributions in other organs including lung, spleen and kidney are different for oral and intravenous administration. For intravenous injection, intact MSNs (AR = 1.5 and 5) were observed in urine by TEM. For oral administration, we did not find any intact MSNs (AR = 1, 1.75 and 5) in urine at 24 h post oral administration. The

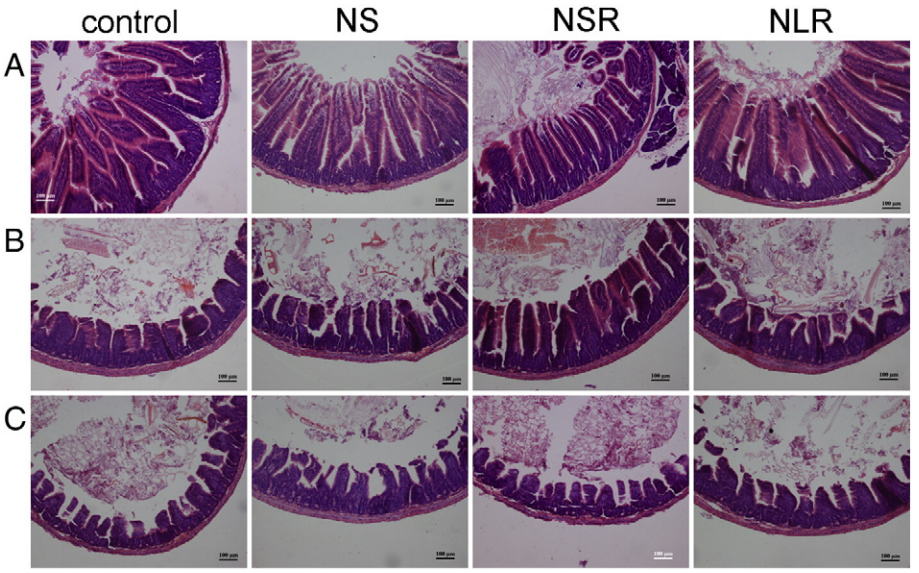

Figure 7. Histological examination of intestine including **(A)** duodenum, **(B)** jejunum and **(C)** ileum for control group, NSs-, NSRs- and NLRs-treated group.

differential shape effect on distribution between intravenous and oral administration may be attributed to two reasons. First, the metabolic pathway of nanoparticles in these two administration routes is totally different. Second, the physical and chemical state of the nanoparticles in different physiological environments is different, which is vital to influencing the dispersity and biodistribution of the nanoparticles. After being administrated by intravenous injection, the particles would be rapidly coated with a layer of opsonin proteins to form nanoparticle-protein corona, which reshapes the surface, charge and resistance to degradation of the nanoparticles[42,43] and further alters their *in vivo* distribution and excretion. Differently, oral administrated MSNs would firstly enter into gastrointestinal tract. The *in vitro* biodegradation test shows that MSNs with three different shapes suffer rapid degradation in the intestinal juice. The partially biodegraded MSNs and/or the degradation products could be absorbed across intestinal mucosal barriers, entering into systematic circulation. The shape-dependent biodegradation and systematic absorption will further lead to different tissue biodistribution and excretion.

The acute toxicity of MSNs was directly related to their biodistribution and excretion. Although the liver, lung, heart and spleen did not show abnormalities for the MSNs-treated groups, the kidneys showed particle shape-dependent tissue damage. The renal toxicity may be attributed to the intact MSNs, degradation product (e.g. irregular small particles) or toxic chemicals released during biodegradation. If the degradation product has a size larger than the renal filtration threshold of about 10 nm,[44] they may be slowly cleared by renal filtration, inducing some damage to the kidney glomerular structure. If they degraded into sub-10 nm particles, smaller than the renal filtration threshold or into small molecules such as orthosilicic acid, they may undergo glomerular filtration and induce some damage to the tissue under high concentration. Yu *et al* found that kidney was the target organ of mesoporous silica intravenous toxicity, irrespective of geometrical features or surface characteristics of the particles.[29] Compared with our previous results of MSNs with the same dose by intravenous injection, which only shows some alternation of CREA and BUN and no obvious histological abnormality of kidney; the damage to kidney was more serious for oral administration. We believe that the biodegradation behavior of MSNs, especially in GIT, which leads to the formation of some toxic chemicals and/or small irregular degradation particles, may be responsible for the kidney damage. These results provide some important insight in understanding the toxicity of MSNs and the effect of biodegradation behavior of these particles. Currently, more comprehensive studies on the mechanism of renal damage after oral and intravenous administrations and the pathway for clearing of the intact MSNs by glomerular filtration are being performed.

In addition, biodegradation rate in gastrointestinal fluids and permeability through intestinal mucous membrane are important aspects in determining the bioavailability of orally administrated drugs. After the drugs are encapsulated into nanoparticles, their biodistribution and absorption may be changed by the physico-chemical properties of the nanoparticles, the interaction between the drugs and the nanoparticles and the *in vivo* distribution and clearance of the nanoparticles. To design effective drug delivery systems, some useful information could be derived from the shape-dependent biodegradation, biodistribution and excretion study of MSNs. The good intestinal absorption and high systematic circulation of the spherical NSs, may be advantageous for drug absorption and bioavailability. Meanwhile, we should pay sufficient attention to the renal toxicity when determining their administration dosage.

In summary, the effects of MSNs with aspect ratio of 1, 1.75 and 5 on their *in vivo* biodistribution, excretion and toxicity after oral administration were studied. With the decrease of aspect ratio, the systematic absorption by small intestine and other organs increased and the urinary excretion decreased. The

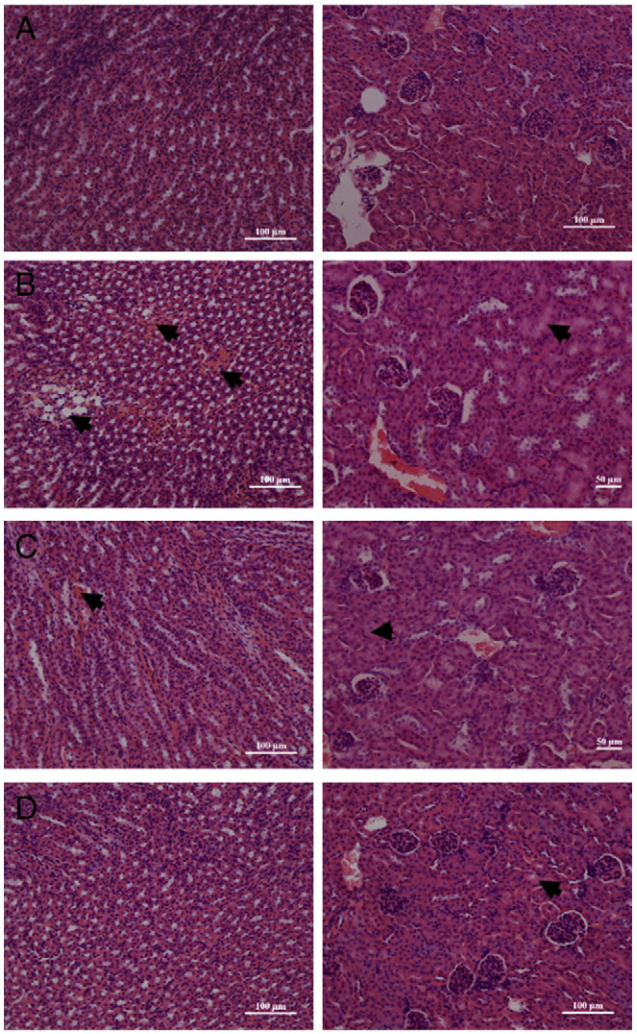

Figure 8. Histological examination of kidney from the mice of **(A)** control group, **(B)** NSs-treated group, **(C)** NSRs-treated group and **(D)** NLRs-treated group. The left column shows the glomeruli and the right column shows the kidney tubules.

tendency of biodistribution is consistent with the degradation rate of the MSNs in simulated body and intestinal fluid. Particle shape dependent renal toxicity of MSNs is observed. These findings would provide some useful information for designing efficient drug delivery systems and for understanding the underlining mechanism of nanotoxicity. Further study will be performed to understand the excretion mechanism from kidney.

Appendix A. Supplementary data

Supplementary data to this article can be found online at http://dx.doi.org/10.1016/j.nano.2015.07.004.

References

1. Peer D, Karp JM, Hong S, FaroKHzad OC, Margalit R, Langer R. Nanocarriers as an emerging platform for cancer therapy. *Nat Nanotechnol* 2007;**2**:751-60.
2. Liong M, Lu J, Kovochich M, Xia T, Ruehm SG, Nel AE, et al. Multifunctional inorganic nanoparticles for imaging, targeting, and drug delivery. *ACS Nano* 2008;**2**:889-96.
3. Nel AE, Madler L, Velegol D, Xia T, Hoek EMV, Somasundaran P, et al. Understanding biophysicochemical interactions at the nano-bio interface. *Nat Mater* 2009;**8**:543-57.
4. Chaturvedi K, Ganguly K, Nadagouda MN, Aminabhavi TM. Polymeric hydrogels for oral insulin delivery. *J Control Release* 2013;**165**:129-38.
5. Almeida AJ, Souto E. Solid lipid nanoparticles as a drug delivery system for peptides and proteins. *Adv Drug Deliv Rev* 2007;**59**:478-90.
6. Li ZX, Barnes JC, Bosoy A, Stoddart JF, Zink JI. Mesoporous silica nanoparticles in biomedical applications. *Chem Soc Rev* 2012;**41**:2590-605.
7. Wang Y, Zhao QF, Han N, Bai L, Li J, Liu J, et al. Mesoporous silica nanoparticles in drug delivery and biomedical applications. *Nanomed Nanotechnol* 2014;**11**:313-27.
8. Wu X, Wu M, Zhao JLXJ. Recent development of silica nanoparticles as delivery vectors for cancer imaging and therapy. *Nanomed Nanotechnol* 2014;**10**:297-312.
9. Barkalina N, Jones C, Kashir J, Coote S, Huang XY, Morrison R, et al. Effects of mesoporous silica nanoparticles upon the function of mammalian sperm *in vitro*. *Nanomed Nanotechnol* 2014;**10**:859-70.
10. Tang FQ, Li LL, Chen D. Mesoporous silica nanoparticles: synthesis, biocompatibility and drug delivery. *Adv Mater* 2012;**24**:1504-34.
11. He Q, Shi J. MSN anti-cancer nanomedicines: chemotherapy enhancement, overcoming of drug resistance, and metastasis inhibition. *Adv Mater* 2014;**26**:391-411.
12. Chen D, Li LL, Tang FQ, Qi S. Facile and scalable synthesis of tailored silica "nanorattle" Structures. *Adv Mater* 2009;**21**:3804-7.
13. Li LL, Tang FQ, Liu HY, Liu TL, Hao NJ, Chen D, et al. *In vivo* delivery of silica nanorattle encapsulated docetaxel for liver cancer therapy with low toxicity and high efficacy. *ACS Nano* 2010;**4**:6874-82.
14. Li LL, Guan YQ, Liu HY, Hao NJ, Liu TL, Meng XW, et al. Silica nanorattle-doxorubicin-anchored mesenchymal stem cells for tumor-tropic therapy. *ACS Nano* 2011;**5**:7462-70.
15. Luo Z, Ding X, Hu Y, Wu S, Xiang Y, Zeng Y, et al. Engineering a hollow nanocontainer platform with multifunctional molecular machines for tumor-targeted therapy *in vitro* and *in vivo*. *ACS Nano* 2013;**7**:10271-84.
16. Du X, Shi BY, Liang J, Bi JX, Dai S, Qiao SZ. Developing functionalized dendrimer-like silica nanoparticles with hierarchical pores as advanced delivery nanocarriers. *Adv Mater* 2013;**25**:5981-5.
17. Lu J, Li ZX, Zink JI, Tamanoi F. *In vivo* tumor suppression efficacy of mesoporous silica nanoparticles-based drug-delivery system: enhanced efficiency by folate modification. *Nanomed Nanotechnol* 2012;**8**:212-20.
18. Lee CH, Lo LW, Mou CY, Yang CS. Synthesis and characterization of positive-charge functionalized mesoporous silica nanoparticles for oral drug delivery of an anti-inflammatory drug. *Adv Funct Mater* 2008;**18**:3283-92.
19. Cheng SH, Liao WN, Chen LM, Lee CH. pH-controllable release using functionalized mesoporous silica nanoparticles as an oral drug delivery system. *J Mater Chem* 2011;**21**:7130-7.
20. Zhang YZ, Wang JC, Bai XY, Jiang TY, Zhang Q, Wang SL. Mesoporous silica nanoparticles for increasing the oral bioavailability and permeation of poorly water soluble drugs. *Mol Pharm* 2012;**9**:505-13.
21. Kupferschmidt N, Xia X, Labrador RH, Atluri R, Ballell L, Garcia-Bennett AE. *In vivo* oral toxicological evaluation of mesoporous silica particles. *Nanomedicine* 2013;**8**:57-64.
22. Decuzzi P, Godin B, Tanaka T, Lee SY, Chiappini C, Liu X, et al. Size and shape effects in the biodistribution of intravascularly injected particles. *J Control Release* 2010;**141**:320-7.
23. Doshi N, Prabhakarpandian B, Rea-Ramsey A, Pant K, Sundaram S, Mitragotri S. Flow and adhesion of drug carriers in blood vessels depend on their shape: a study using model synthetic microvascular networks. *J Control Release* 2010;**146**:196-200.
24. Chaudhuri P, Harfouche R, Soni S, Hentschel DM, Sengupta S. Shape effect of carbon nanovectors on angiogenesis. *ACS Nano* 2010;**4**:574-82.

25. Geng Y, Dalhaimer P, Cai SS, Tsai R, Tewari M, Minko T, et al. Shape effects of filaments versus spherical particles in flow and drug delivery. *Nat Nanotechnol* 2007;**2**:249-55.
26. Champion JA, Mitragotri S. Role of target geometry in phagocytosis. *Proc Natl Acad Sci U S A* 2006;**103**:4930-4.
27. Chauhan VP, Popovic Z, Chen O, Cui J, Fukumura D, Bawendi MG, et al. Fluorescent nanorods and nanospheres for real-time *in vivo* probing of nanoparticle shape-dependent tumor penetration. *Angew Chem Int Ed* 2011;**50**:11417-20.
28. Meng H, Yang S, Li ZX, Xia T, Chen J, Ji ZX, et al. Aspect ratio determines the quantity of mesoporous silica nanoparticle uptake by a small GTPase-dependent macropinocytosis mechanism. *ACS Nano* 2011;**5**:4434-47.
29. Yu T, Greish K, McGill LD, Ray A, Ghandehari H. Influence of geometry, porosity, and surface characteristics of silica nanoparticles on acute toxicity: their vasculature effect and tolerance threshold. *ACS Nano* 2012;**6**:2289-301.
30. Huang XL, Li LL, Liu TL, Hao NJ, Liu HY, Chen D, et al. The shape effect of mesoporous silica nanoparticles on biodistribution, clearance, and biocompatibility *in vivo*. *ACS Nano* 2011;**5**:5390-9.
31. Hao NJ, Liu HY, Li LL, Chen D, Li LF, Tang FQ. *In vitro* degradation behavior of silica nanoparticles under physiological conditions. *J Nanosci Nanotechnol* 2012;**12**:6346-54.
32. Marques MRC, Loebenberg R, Almukainzi M. Simulated biological fluids with possible application in dissolution testing. *Dissolut Technol* 2011;**18**:15-28.
33. Liu TL, Li LL, Teng X, Huang XL, Liu HY, Chen D, et al. Single and repeated dose toxicity of mesoporous hollow silica nanoparticles in intravenously exposed mice. *Biomaterials* 2011;**32**:1657-68.
34. Gu JL, Huang M, Liu JP, Li YS, Zhao WR, Shi JL. Calcium doped mesoporous silica nanoparticles as efficient alendronate delivery vehicles. *N J Chem* 2012;**36**:1717-20.
35. Yamada H, Urata C, Aoyama Y, Osada S, Yamauchi Y, Kuroda K. Preparation of colloidal mesoporous silica nanoparticles with different diameters and their unique degradation behavior in static aqueous systems. *Chem Mater* 2012;**24**:1462-71.
36. Zhang SL, Chu ZQ, Yin C, Zhang CY, Lin G, Li Q. Controllable drug release and simultaneously carrier decomposition of SiO_2-drug composite nanoparticles. *J Am Chem Soc* 2013;**135**:5709-16.
37. Ensign LM, Cone R, Hanes J. Oral drug delivery with polymeric nanoparticles: the gastrointestinal mucus barriers. *Adv Drug Deliv Rev* 2012;**64**:557-70.
38. Powell JJ, Faria N, Thomas-McKay E, Pele LC. Origin and fate of dietary nanoparticles and microparticles in the gastrointestinal tract. *J Autoimmun* 2010;**34**:J226-33.
39. Schleh C, Semmler-Behnke M, Lipka J, Wenk A, Hirn S, Schaffler M, et al. Size and surface charge of gold nanoparticles determine absorption across intestinal barriers and accumulation in secondary target organs after oral administration. *Nanotoxicology* 2012;**6**:36-46.
40. Eldridge JH, Hammond CJ, Meulbroek JA, Staas JK, Gilley RM, Tice TR. Controlled vaccine release in the gut-associated lymphoid-tissues. 1. Orally-administered biodegradable microspheres target the Peyer's patches. *J Control Release* 1990;**11**:205-14.
41. Jani P, Halbert GW, Langridge J, Florence AT. The uptake and translocation of latex nanospheres and microspheres after oral-administration to rats. *J Pharm Pharmacol* 1989;**41**:809-12.
42. Cedervall T, Lynch I, Lindman S, Berggard T, Thulin E, Nilsson H, et al. Understanding the nanoparticle-protein corona using methods to quantify exchange rates and affinities of proteins for nanoparticles. *Proc Natl Acad Sci U S A* 2007;**104**:2050-5.
43. Mahmoudi M, Lynch I, Ejtehadi MR, Monopoli MP, Bombelli FB, Laurent S. Protein-nanoparticle interactions: opportunities and challenges. *Chem Rev* 2011;**111**:5610-37.
44. Choi HS, Liu W, Misra P, Tanaka E, Zimmer JP, Ipe BI, et al. Renal clearance of quantum dots. *Nat Biotechnol* 2007;**25**:1165-70.